

On the analysis of vertical shafts in soft ground: Evaluating Soil-Structure Interaction Using Two Different Numerical Modeling Techniques

Viet D.H. Tran

Graduate student, McGill University, Montreal, QC, Canada

Thamer E. Yacoub

Rocscience, Inc., Toronto, ON, Canada

Mohamed A. Meguid

Department of Civil Engineering-McGill University, Montreal, QC, Canada

ABSTRACT

The soil-structure interaction developing due to the construction of vertical shafts in soft ground is numerically investigated in this study using the finite and discrete element methods. An axisymmetric joint element is utilized to model the interaction between the shaft lining and the surrounding soil using axisymmetric finite element method. The results are compared with those obtained using discrete element analysis where the soil domain is modeled using discrete particles while the shaft is modeled as a rigid cylinder. The effect of soil displacement in the vicinity of the shaft lining was examined by incrementally reducing the shaft diameter and calculating the pressure acting on the shaft as well as the stress distribution in soil. Results obtained from the two methods are then compared and conclusions are made regarding the sufficiency of these methods to analyze similar axisymmetric geotechnical engineering problems.

RÉSUMÉ

Dans cette étude, l'interaction sol-structure, causé par la construction de puits verticaux dans le sol, est examinée de façon numérique grâce à la méthode des éléments finis ainsi que la méthode des éléments discrets. Un élément de joint axisymétrique est utilisé pour modéliser l'interaction entre le revêtement du puits et le sol avoisinant en employant la méthode des éléments finis axisymétrique. Les résultats sont comparés avec ceux obtenus avec la méthode des éléments discrets ou le domaine du sol est modélisé en utilisant des particules discrètes tandis que le puits est modélisé comme étant un cylindre rigide. L'effet du déplacement du sol à proximité du revêtement du puits est examiné en prenant en considération une réduction incrémentale du diamètre du puits, le calcul de la pression exercée sur le puits ainsi que la répartition des contraintes dans le sol. Les résultats obtenus pour les deux méthodes sont, ensuite, comparés et des conclusions sont émises concernant la suffisance de ces méthodes à analyser des problèmes similaires d'axisymétrie géotechnique.

1 INTRODUCTION

Evaluating earth pressure on vertical shafts and stress distributions in the surrounding soil have received extensive research interest in the past few decades. This is due to the fact that earth pressure acting on cylindrical walls does not generally follow the conventional analytical solutions used for plane strain analysis. Experimental studies that examined pressure distribution around vertical shafts have been reported in the literature including Walz (1973), Lade et al. (1981), König et al. (1991), Chun and Shin (2006) and Tobar and Meguid (2011). Theoretical solutions emphasizing 3D arching around shaft linings have also been reported such as Cheng and Hu (2005); Cheng et al. (2007); Salgado and Prezzi (2007); Andresen et al. (2010) and Osman and Randolph (2012). Beside experimental and analytical analyses, numerical approaches such as Finite element method (FEM) and Discrete element method (DEM) have been used to model the behavior of shaft systems. FE simulations reported by Wong and Kaiser (1988) and Wang et al. (1997) did not properly consider the interface behavior between the shaft and surrounding soil. The Discrete element method (DEM) proposed by Cundall and Strack (1979) has proven to be a promising approach to

capture the response of granular materials. An attempt has been made by Herten and Pulsfort (1999) to apply the DEM to simulate a laboratory size shaft construction. Although the study provided useful results, the circular shaft was assumed to behave as a small flat wall which has led to an inadequate simulation of the arching effect and the stress distribution around the shaft. Therefore, there is a need for an improved DE simulation of the problem considering the problem geometry as well as realistic soil properties.

The two numerical methods, FEM and DEM, are used in this paper to analyze the soil-shaft interaction problem. In the first approach, an axisymmetric finite element analysis is implemented to model the interaction between the shaft lining and the surrounding soil using a newly developed axisymmetric joint element. In the second approach, the soil domain is modeled using DE particles while the shaft is modeled as a rigid cylinder. The results of the two numerical approaches regarding the pressures acting on the shaft and stress distributions in soil around the shaft are analyzed. The efficiency of the two methods in modeling this geotechnical engineering problem is also discussed.

2 NUMERICAL SIMULATION

2.1 FEM Simulation

This study examines the earth pressure acting on a rigid shaft and stress distribution in the surrounding soil. The shaft has a diameter of 0.15m and a height of 1.0m embedded in a thick cohesionless sand layer. The geometry of the modeled problem is shown in Figure 1.

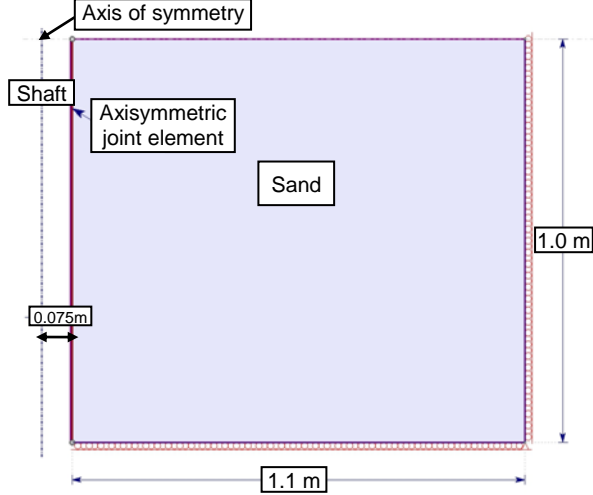


Figure 1. Model of an axisymmetric vertical shaft

Due to the axisymmetry in loading and geometry, an axisymmetric model has been selected for the shaft analysis. The interaction between the shaft and surrounding soil is modeled using a developed axisymmetric joint element. The formulation of the axisymmetric joint element (Goodman et al., 1968; Yuan and Chua, 1992) has been implemented in the FE program Phase² (Rocscience, 2012) and is summarized below:

Strain - Displacement matrix:

Let u and v be the relative displacements along the local coordinates ξ and η ; u_i and v_i be the nodal displacements in the local coordinate system (Figure 2). Let γ and ε be the joint shear strain and joint normal strain in the local coordinate system, t be the thickness of the joint element, which is very small compared to the length of the joint.

$$\gamma = \frac{\partial u}{\partial \eta} + \frac{\partial v}{\partial \xi} \cong \frac{u}{t} \quad [1]$$

$$\varepsilon = \frac{\partial v}{\partial \eta} \cong \frac{v}{t} \quad [2]$$

From (1) and (2):

$$\begin{Bmatrix} \gamma \\ \varepsilon \end{Bmatrix} = \frac{1}{t} \begin{Bmatrix} u \\ v \end{Bmatrix} \quad [3]$$

Eq. 3 can be rewritten as:

$$\begin{Bmatrix} \gamma \\ \varepsilon \end{Bmatrix} = \mathbf{B} \mathbf{u} \quad [4]$$

Where \mathbf{B} is the strain – displacement matrix, \mathbf{u} is the displacement vector.

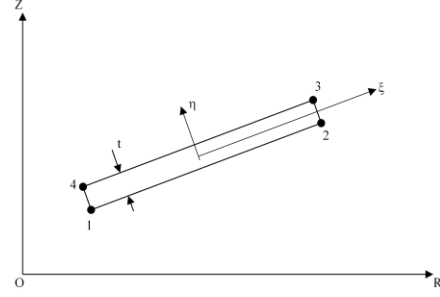


Figure 2. A four –node axisymmetric joint element

Elastic constitutive matrix:

Note that the joint element represents the interaction between two finite elements and is not a material itself, therefore only the normal and tangential stresses exist.

$$\begin{Bmatrix} \tau \\ \sigma \end{Bmatrix} = \mathbf{D} \begin{Bmatrix} \gamma \\ \varepsilon \end{Bmatrix} \quad [5]$$

where:

$$\mathbf{D} = \begin{bmatrix} k_s t & 0 \\ 0 & k_n t \end{bmatrix} \quad [6]$$

In Eq. 6, k_n and k_s are the normal and shear stiffnesses of the joint, respectively. By eliminating the term thickness t , the elastic constitutive matrix becomes:

$$\mathbf{D} = \begin{bmatrix} k_s & 0 \\ 0 & k_n \end{bmatrix} \quad [7]$$

Element stiffness matrix:

The element stiffness matrix in the local coordinate system:

$$\mathbf{K} = \int_{-1}^1 \mathbf{B}^T \mathbf{D} \mathbf{B} R \theta d\xi \quad [8]$$

where θ is the circumferential angle, and R is the radial distance in the global coordinate system.

If θ is one radian, (8) becomes:

$$\mathbf{K} = \int_{-1}^1 \mathbf{B}^T \mathbf{D} \mathbf{B} R \cdot \xi \quad [9]$$

The element stiffness matrix can be numerically calculated by:

$$\mathbf{K} = \sum_{I=1}^{NIP} J \cdot R_I \cdot W(I) \cdot \mathbf{B}^T \mathbf{D} \mathbf{B}_I \quad [10]$$

Where NIP is the number of Gauss points, $W(I)$ is the weighting coefficient in accordance with the Gauss point i^{th} , J is the Jacobian determinant.

In this study, the sand material reported in Tran et al. (2012) is used for the simulation. The peak friction angle of the axisymmetric joint element is determined to be the same as that of the sand. A parametric study was

conducted to examine the effect of the joint stiffnesses on the shaft-soil interaction. Results indicated that the joint stiffnesses do not have a significant effect on the simulation results. The material parameters of the joint element and sand layer are shown in Table 1. Active lateral earth pressures on the shaft and stresses in the soil domain are obtained by slightly moving inward the shaft lining.

Table 1. Material properties in the FE simulation

Sand material		Joint material	
Unit weight (kN/m ³)	14.7	Normal stiffness (kPa/m)	100000
Young's Modulus (kPa)	20000	Shear stiffness (kPa/m)	10000
Poisson's ratio	0.35	Tensile strength (kPa)	0
Failure criterion	Mohr-Coulomb	Slip criterion	Mohr-Coulomb
Friction angle (peak) (deg)	41	Peak friction angle (deg)	41
Cohesion (kPa)	0	Peak cohesion (kPa)	0

2.2 DEM Simulation

DEM Formulation:

The discrete element method, generally, considers the interaction between distinct particles at their contact points. The interaction between particles is usually regarded as a dynamic process that reaches static equilibrium when the internal forces are balanced. The dynamic behavior is represented by a time-step algorithm using an explicit time-difference scheme. Newton's equations of motion are then used to determine particle displacement.

The DEM simulations in this study are conducted using YADE, an open source discrete element code (Kozicki and Donze 2009, Šmilauer et al. 2010). Spherical particles of different sizes are used to represent an idealized granular material. The contact law between particles is briefly described below (Figure 3):

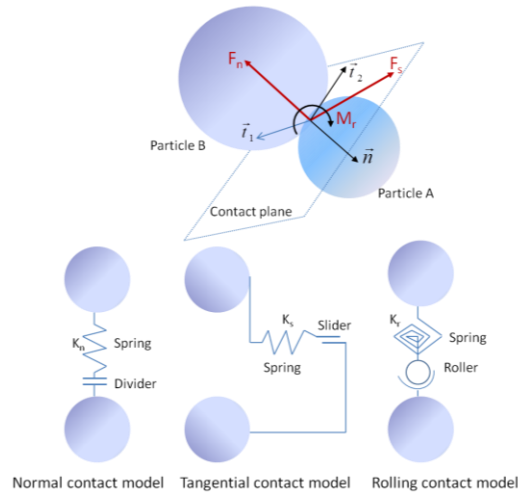


Figure 3. Interaction between two DE particles

If two particles A and B with radii r_A and r_B are in contact, the contact penetration depth is defined as:

$$\Delta = r_A + r_B - d_0 \quad [11]$$

where d_0 is the distance between the two centers of particle A and B.

The force vector \vec{F} which represents the interaction between the two particles is decomposed into normal and tangential forces:

$$\vec{F}_N = K_N \cdot \vec{\Delta}_N, \quad \delta \vec{F}_T = -K_T \cdot \delta \vec{\Delta}_T \quad [12a,b]$$

Where \vec{F}_N and \vec{F}_T are the normal and tangential forces; K_N and K_T are the normal and tangential stiffnesses at the contact; $\delta \vec{\Delta}_T$ is the incremental tangential displacement and $\vec{\Delta}_N$ is the normal penetration between the two particles. K_N and K_T are defined by:

$$K_N = \frac{2E_A r_A E_B r_B}{E_A r_A + E_B r_B} \quad [13]$$

where E is the particle material modulus. The interaction tangential stiffness K_T is determined as a given fraction of the computed K_N . The macroscopic Poisson's ratio is determined by the K_T/K_N ratio while the macroscopic Young's modulus is proportional to K_N and affected by K_T/K_N .

The tangential force \vec{F}_T is limited by a threshold value such that:

$$\vec{F}_T = \frac{\vec{F}_T}{\|\vec{F}_T\|} \|\vec{F}_N\| \tan(\varphi_{micro}) \text{ if } \|\vec{F}_T\| \geq \|\vec{F}_N\| \tan(\varphi_{micro}) \quad [14]$$

where φ_{micro} is the microscopic friction angle.

To represent the rolling behavior between two particles A and B, a rolling angular vector $\vec{\theta}_r$ is used. This vector describes the relative orientation change between the two particles. A resistant moment \vec{M}_r resulting from this change is computed by:

$$\vec{M}_r = \begin{cases} K_r \vec{\theta}_r & \text{if } K_r \|\vec{\theta}_r\| < \|\vec{M}_r\|_{lim} \\ \|\vec{M}_r\|_{lim} \frac{\vec{\theta}_r}{\|\vec{\theta}_r\|} & \text{if } K_r \|\vec{\theta}_r\| \geq \|\vec{M}_r\|_{lim} \end{cases} \quad [15]$$

where:

$$\|\vec{M}_r\|_{lim} = \eta_r \|\vec{F}_N\| \frac{r_A + r_B}{2} \quad [16]$$

K_r is the rolling stiffness of the interaction computed by:

$$K_r = \beta_r \left(\frac{r_A + r_B}{2} \right)^2 K_T \quad [17]$$

where β_r is the rolling resistance coefficient and η_r is a dimensionless coefficient.

To record macroscopic stress components within a representative volume V , the following equation is used:

$$\sigma_{ij} = \frac{1}{V} \sum_{c=1}^{N_c} x^{c,i} f^{c,j} \quad [18]$$

where N_c is the number of contacts within the volume V , $f^{c,j}$ is the contact force vector at contact c , $x^{c,i}$ is the branch vector connecting two contact particles A and B , and indices i and j indicate the Cartesian coordinates.

Shaft simulation:

The vertical shaft is modeled using a cylinder 1.0 m in height and initial diameter of 0.15 m that comprises 12 equally distributed segments. Since the modeled problem is axisymmetric, only part of the domain is modeled to reduce the computational cost. In addition, better representation of the problem can be achieved by simulating one "slice" of the soil domain with a large number of particles while keeping the simulation time acceptable. To capture the problem geometry, a quarter of the problem is modeled in this study. The model consists of a quarter of the shaft and four boundaries including three vertical and one horizontal at the bottom of the container (Figure 4). Each quarter of the shaft is divided into three segments to capture the curved shaft geometry. Pressures acting on the shaft are recorded at the middle segment to reduce the boundary effects.

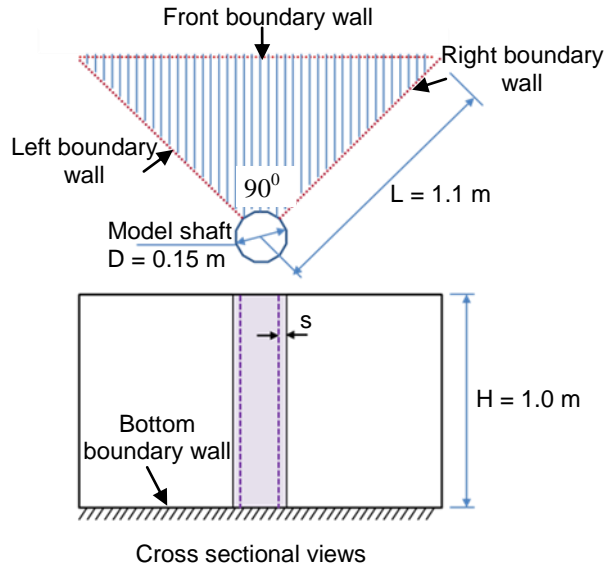


Figure 4. DEM model of the shaft problem

The DE soil domain is generated using the multi-layer packing technique proposed by Tran et al. (2012). The packing procedure is described as follows:

The number of layers is first chosen (ten layers in this study) and the volume of particles for each layer is

calculated based on the target void ratio of the final soil specimen (which is 0.39). To generate the first layer, a set of non-contacting particles is first generated inside a box following a pre-determined particle size distribution until the target volume is reached. The height of the box is chosen to be larger than the target height of the layer to insure that all particles can be generated without overlapping. Gravity is then applied to all particles allowing them to move downward and come in contact with each other. The interparticle friction angle is set to zero. To increase the density of the packing, lateral shaking movement is applied to the box to help small particles move into voids between larger particles. The first layer generation is completed when the system reaches equilibrium. For the second layer, the height of the box is increased and the second "cloud" of non-contacting particles is generated in the area above the existing particles. Gravity and shaking are then applied and the system is allowed to come into equilibrium. The procedure is repeated until the final specimen is formed. The proposed multi-layer approach helps increase the density of the packing while keeping the packing pattern realistic.

The behavior of a DE specimen depends not only on the packing structure but also on the particle size distribution. However, the true replication of grain size is usually restricted by the high computational cost caused by the large number of particles. In this study, particles smaller than D_5 (particle diameter corresponding to 5% passing) are neglected to reduce the computational time. This is appropriate as these particles are assumed to have minor effect on the force chains that transmit stresses within the sample (Calvetti 2008, Cheung 2010). For the simulation of large scale problems, particle up-scaling is often used to reduce the number of modeled particles. Careful consideration of particle sizes is usually made to keep balance between the computational cost and the scaling effects on the sample responses. In this study, the scale factors (ratio of a numerical particle size to its real particle size) are chosen as 25 for the simulation. The particle size distribution used in the simulation is shown in Table 2.

Table 2. Grain size distributions in the DE simulation

Sieve diameter (mm)	% passing (weight)
6	0
10	22
21	45
25	100

The properties of DE particles are determined from calibration tests using the direct shear test as reported in Tran et al. (2012). A summary of the DE parameters is given in Table 3. The diameter of the shaft is incrementally reduced to model the active condition. Lateral earth pressures on the shaft and stresses in the soil domain are recorded at different wall movements. As reported in Tran et al. (2012), the required wall movement to activate the pressure on shafts is less than 0.5% of the shaft height. Therefore, the simulation process finishes when the reduction in the shaft radius reaches 5 mm.

Table 3. Particles' properties for DE simulation

Parameter	Value
Particle density (kg/m ³)	2650
Particle material modulus E (MPa)	38
Ratio K_T/K_N	0.25
Friction angle φ (degrees)	34
β_R	0.05
η_R	1

3 RESULTS AND DISCUSSIONS

The earth pressure distributions on the shaft obtained using FE and DE simulations are presented in Figure 5. The numerical results are also compared with analytical solutions reported by Terzaghi (1943), Berezantzev (1958), and Cheng and Hu (2005). The FE simulation provided the active pressure on the shaft with a small shaft lining movement (less than 1 mm in this study) whereas the DE simulation provided the pressure distributions with different shaft movements. It can be seen from the DE simulation that when the shaft movement increased, pressures acting on the shaft reduced. The pressure distributions following the solutions of Terzaghi and Berezantzev are in good agreement with the numerical results provided that enough wall movement is allowed. A good agreement between the FE and DE simulations results at a shaft movement of 4 mm is also observed.

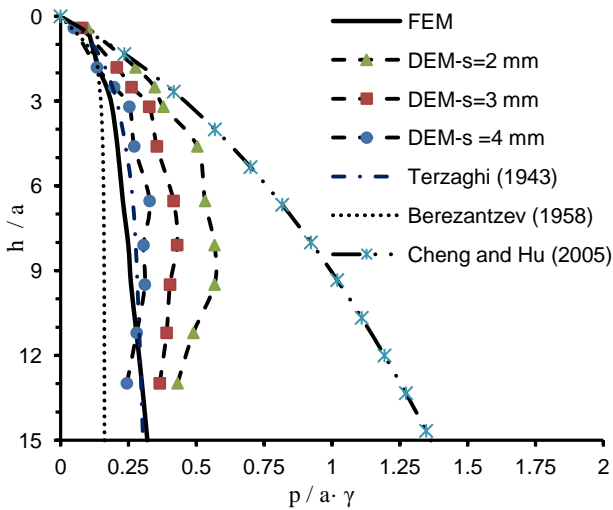


Figure 5. Pressure distributions along the shaft

Figure 6 shows the displacement fields around the shaft for both the FE and DE simulations. It can be seen that a non-uniform failure zone of conical shape has developed along the shaft. The zone increased in size from the bottom of the shaft up to a region of 0.2 m in radius at the surface (about 2.5 times the shaft radius).

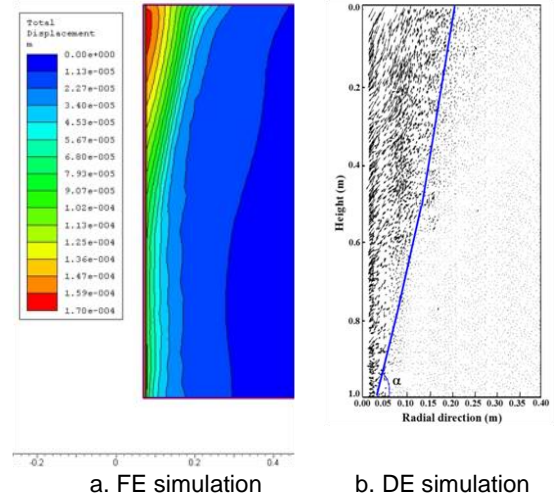


Figure 6. Pressure distributions along the shaft

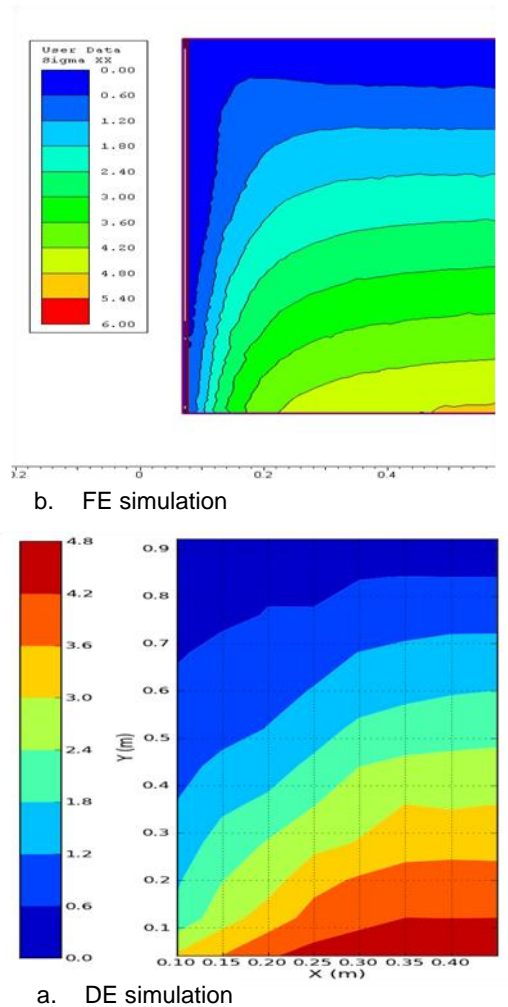
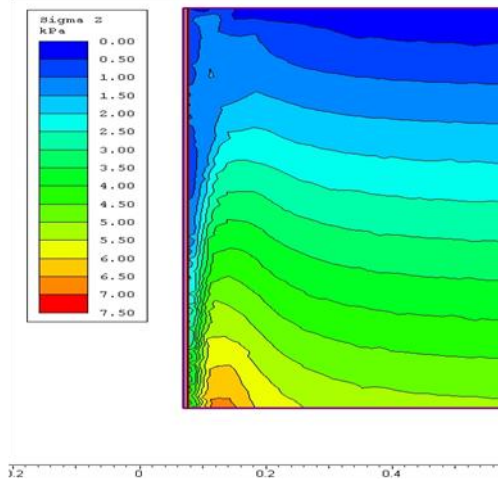
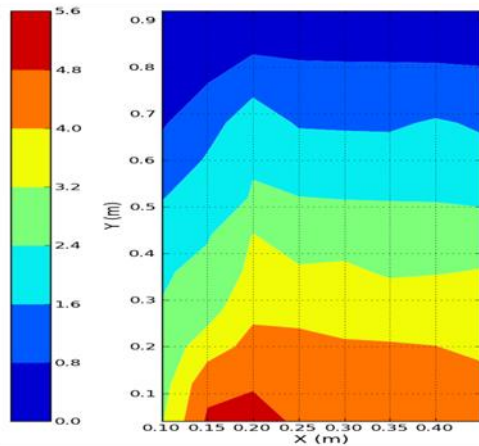


Figure 7. Radial stress distribution in soil



a. FE simulation



b. DE simulation

Figure 8. Circumferential stress distribution in soil

The radial and circumferential stresses in soil are shown in Figure 7 and 8. It can be seen from both FE and DE simulations that the radial stress near the shaft wall dropped rapidly and the change in radial stress mostly occurred within 0.3 m from the center of the shaft. The stress outside this region remained close to its initial state (Figure 7). The relief of radial stresses due to soil movement causes vertical (along the shaft height) and horizontal (in the circumferential direction) arching, and results in stress redistribution in the vicinity of the shaft. It is observed from Figure 8 that the circumferential stress near the shaft was smaller than the initial value. The circumferential stresses increased with distance from the shaft due to horizontal arching. At a distance of about 0.15 m from the shaft center, the circumferential stress reached a maximum value which is larger than the initial value. A decreasing trend is observed with further increase in distance and the circumferential stress returns to its initial state far away from the shaft (Figure 8). The soil displacement as well as stress distributions in soil show a good agreement with previous studies (Berezantzev, 1958; Cheng and Hu, 2005, Tobar and Meguid, 2011; Tran et al., 2012). It can be observed that

good agreement results were achieved using FE and DE simulations.

4 SUMMARY AND CONCLUSIONS

In this paper, two numerical modeling techniques, FEM and DEM, were used to investigate the lateral earth pressure acting on a cylindrical shaft and the stresses in the surrounding soil. In the FE approach, an axisymmetric joint element was utilized to model the interaction between the shaft lining and the surrounding soil using an axisymmetric finite element method. In the DE approach, the soil domain was modeled using discrete particles while the shaft is modeled as a rigid cylinder. The results of the FE and DE simulations including pressure acting on the shaft and stress distributions in soil were analyzed.

Lateral pressure along the shaft obtained from both the FE and DE analyses agreed well with the analytical solutions proposed by Terzaghi and Berezantzev. Both the FE and DE simulations confirmed a non-uniform failure zone of conical shape along the shaft. The zone increased in size from the bottom of the shaft up to a region of about 2.5 times the shaft radius at the surface. The movement of the shaft wall resulted in a redistribution of stresses within the soil medium. The arching effect had lead to a decrease in radial stresses and increase in circumferential stresses within a region of radius 0.3 m from the shaft center. The FE simulation results presented a good agreement with the DE simulation. The study demonstrated the efficiency of using the FE and DE approaches in simulating vertical shaft problems involving granular material.

ACKNOWLEDGEMENTS

This research is supported by a research grant from the Natural Sciences and Engineering Research Council of Canada (NSERC). The authors also wish to acknowledge Rocscience Inc. for providing the finite element analytical tool.

REFERENCES

- Andresen, L., Jostad, H. P, and Andersen, K. H. 2010. Finite element analyses applied in design of foundations and anchors for offshore structures, *International Journal of Geomechanics*, 11(6), 417-430.
- Berezantzev, V. G. 1958. Earth pressure on the cylindrical retaining walls, *Conference on earth pressure problems*, Brussels, 21-27.
- Calvetti, F. 2008. Discrete modelling of granular materials and geotechnical problems, *European Journal of Environmental and Civil Engineering*, 12: 951-965.
- Cheng, Y. M., and Hu, Y. Y. 2005. Active earth pressure on circular shaft lining obtained by simplified slip line solution with general tangential stress coefficient, *Chinese Journal of Geotechnical Engineering*, 27(1), 110-115.
- Cheng, Y. M., Hu, Y. Y., and Wei, W.B. 2007. General Axisymmetric Active Earth Pressure by Method of

- Characteristics—Theory and Numerical Formulation, *International Journal of Geomechanics*, 7(1), 1-15.
- Cheung, G. 2010. Micromechanics of sand production in oil wells, *Ph.D thesis*, Imperial College London.
- Chun, B., and Shin, Y. 2006. Active earth pressure acting on the cylindrical retaining wall of a shaft, *South Korea Ground and Environmental Engineering Journal*, 7(4): 15-24.
- Cundall. P. A, and Strack O. D. L 1979. A discrete numerical model for granular assemblies, *Géotechnique*, 29(1): 47-65.
- Goodman, Richard E., Robert L. Taylor, and Tor L. Brekke. 1968. A model for the mechanics of jointed rock, *Journal of Soil Mechanics & Foundations Division*.
- Herten, M., and Pulsfort, M. 1999. Determination of spatial earth pressure on circular shaft constructions, *Granular Matter*, 2(1): 1-7.
- Konig, D., Guettler, U., and Jessberger, H. L. 1991. Stress redistribution during tunnel and shaft construction, *Proceedings of the International Conference Centrifuge 1991*, Boulder, Colorado, 129-135.
- Kozicki, J., and Donze, V. F. 2009. YADE-OPEN DEM: an open-source software using a discrete element method to simulate granular material, *Engineering Computations*, 26(7): 786 – 805.
- Lade, P. V., Jessberger, H. L., Makowski, E., and Jordan, P. 1981. Modeling of deep shafts in centrifuge test, *Proceedings of the International Conference on Soil Mechanics and Foundation Engineering*, Stockholm, Sweden, Vol. 1, pp 683-691.
- Osman, A. S., and Randolph, M. F. 2012. Analytical solution for the consolidation around a laterally loaded pile, *International Journal of Geomechanics*, 12(3), 199-208.
- Rocscience. 2012. Rocscience Phase² User's Guide, *Rocscience Inc.*, Toronto, Ontario, Canada.
- Salgado, M., and Prezzi, M. 2007. Computation of Cavity Expansion Pressure and Penetration Resistance in Sands, *International Journal of Geomechanics*, 7(4), 251-265.
- Šmilauer, V., Catalano, E., Chareyre, B., Dorofeenko, S., Duriez, J., Gladky, A., Kozicki, J., Modenese, C., Scholtès, L., Sibille, L., Stránský, J., and Thoeni, K. 2010. *Yade Documentation*, The Yade Project 2010. (<http://yade-dem.org/doc/>).
- Terzaghi, K. 1943. Theoretical soil mechanics, *New York: John Wiley & sons Inc.*
- Tobar, T., and Meguid, M. A. 2011. Experimental study of the earth pressure distribution on cylindrical shafts, *ASCE Journal of Geotechnical and Geoenvironmental Engineering*, 137(11): 1121-1125.
- Tran, V. D., Meguid, M. A., & Chouinard, L. E. 2012. Discrete Element and Experimental Investigations of the Earth Pressure Distribution on Cylindrical Shafts, *International Journal of Geomechanics* (in press).
- Walz, B. 1973. Left bracket apparatus for measuring the three-dimensional active soil pressure on a round model caisson right bracket, *Baumaschine und Bautechnik*, 20(9): 339-344 (in German).
- Wang, S.H., Li, W. and Wang, Y. 1997. A finite element simulation to the process of excavation of a circular retaining wall, *Harbor Engineering* (in Chinese), (3), 30-33.
- Wong, R. C. K., & Kaiser, P. K. 1988. Behaviour of vertical shafts: reevaluation of model test results and evaluation of field measurements, *Canadian Geotechnical Journal*, 25(2), 338-352.
- Yuan, Z., and Chua, K. M. 1992. Exact formulation of axisymmetric-interface-element stiffness matrix, *Journal of geotechnical engineering*, 118(8), 1264-1271.